**52nd AIAA/ASME/ASCE/AHS/ASC Structures, Structural Dynamics and Materials Conference
 19th**
4 - 7 April 2011, Denver, Colorado

AIAA 2011-1928

Computational Engineering of Mixed-mode, In-plane Crack Propagation in Laminated Fiber Reinforced Composites

Siva Shankar Rudraraju,[*] Amit Salvi,[†] Krishna Garikipati,[‡] and Anthony M. Waas [§]

University of Michigan, Ann Arbor, MI 48109, USA

Integrated Computational Engineering (ICE) is a valuable and cost effective resource for ensuring structural integrity and damage tolerance of future aerospace vehicles that are made with laminated fiber reinforced composite laminates. Towards that end, the variational multiscale cohesive method (VMCM) reported by the authors in previous AIAA SDM conferences,[23–26] is extended further to address problems of mixed mode in-plane crack propagation in fiber reinforced laminates. A set of experimental results obtained using a single edge notch eccentric three point bend test is used for validating the VMCM predictions. Further the applicability of VMCM is demonstrated through simulation of mixed mode in-plane crack propagation for different specimen geometries and different loading conditions.

I.   Introduction

A large number of tests, which can contribute to a substantial portion of the total design and manufacturing cost of an aerospace vehicle, are required to ensure the structural integrity and damage tolerance of vehicle structures. These costs can be reduced by developing validated and physics based computational models that can exploit the power of advanced simulation techniques and the increasing computational power of digital computers. High fidelity computational models can provide valuable information regarding the performance of a structure upto and including failure, provided the modeling is based on correct physics, and is validated using laboratory tests that are designed to be discriminatory. The field of integrated computational engineering (ICE), that encompasses this activity, and also includes, in the case of composites, the modeling of the manufacturing process[14] is a rapidly growing and indispensable field which will continue to provide new insights into the performance of advanced composite structures.

The finite element method (FEM), is a key enabler of ICE. It has become the mainstay of problems involving any of the broad phenomena of material deformation - elasticity, plasticity and damage. However, its utility for problems of crack propagation has met with mixed success. The distinguishing characteristic of crack problems, in general, is the formation and propagation of sharp boundaries, which are not part of the original boundary value problem. This is not an obstacle, if the resulting crack path is known a priori, and the mesh is ensured to have elemental surfaces align along possible crack surfaces; but often in practice, neither conditions are feasible. For all but trivial crack propagation problems, the crack path is not known beforehand and has to be determined as part of the solution process, and in structural level problems adaptive mesh generation/realignment is prohibitively costly. The traditional Galerkin FEM implementation is not suitable for problems that encounter crack propagation and also involve strain localization, as it leads to mesh subjective schemes, and the related limitations have been well documented in the context of spurious mesh related length scales[1, 4, 9] and requirements of mesh alignment relative to the localization

---

[*]Graduate Student, Department of Mechanical Engineering, 2350 Hayward Street, Ann Arbor, MI 48109, USA.

[†]Research Fellow, Department of Aerospace Engineering, 1320 Beal Avenue, Ann Arbor, MI 48109, USA.

[‡]Associate Professor, Department of Mechanical Engineering, 2350 Hayward Street, Ann Arbor, MI 48109, USA.

[§]Felix Pawlowski Collegiate Professor of Aerospace Engineering, Department of Aerospace Engineering, 1320 Beal Avenue, Ann Arbor, MI 48109, USA. Fellow AIAA.

American Institute of Aeronautics and Astronautics

band.[17, 22]Further in the context of cracks, the "global" non-linearity of the load response which depends on the microstructure of the material, also requires new constitutive relations which can span across different length scales. These additional cohesive relations between the crack face opening and its internal tractions, referred to as traction-separation relations (Figure 1), lead to the more challenging class of cohesive cracks and bridging cracks, where the crack surface may be a diffused zone of damage rather than a sharp boundary.

Consider the case of through-the-thickness crack propagation in fiber-reinforced composites. Because of the different length scales associated with the microstructure of a composite material and the resulting composite structure, a multitude of failure mechanisms can be simultaneously operative, leading to a very complex damage progression in a composite structure. A sharp, through the thickness crack can be present in these composites initially, but, as soon as local damage (possibly in the form of matrix micro-cracking) accumulates, crack blunting and distributed damage occurs across the highly stressed areas around the initial crack tip. As this initial crack starts to grow, a damaged zone of material (bridging zone) evolves in the wake of the instantaneous crack tip. Thus, unlike in monolithic materials, such as metals, there is no well defined "crack" that can be identified. Instead, a diffused zone of damage is seen to advance. This distributed damage results in additional resistance to advancing damage growth, largely contributed by fiber bridging and pullout in the crack wake . This enhanced fracture resistance is desirable and is a major contributor to the increased toughness of these laminated composites.[2, 3, 7, 8, 25] But for the analytical treatment, these microstructural mechanisms often give rise to a process zone that is considerably larger than that permitted for the application of linear elastic fracture mechanics (LEFM) models, and the material non-linearity that is induced by these mechanisms leads to a relief of the singular fields at the mathematically sharp crack tip, that would otherwise persist in a strict LEFM setting of an elastic material. In this context, cohesive zone models, which embed process zone mechanics through nonlinear traction-separation relationships across the crack faces become an important tool for analysis.[5, 21, 27, 30, 33, 35–37] However the numerical implementation of cohesive zone modeling is often through surface elements which need to be placed along intended crack paths, limiting crack growth studies to cases where a-priori information of the crack path is known. This major limitation can be overcome by developing continuum elements that can simultaneously be used for both continuum and non-continuum (severed by a crack or cracks, leading to a discontinuity in the displacement field) modeling. Thus the primary task of this paper is presenting the variational multiscale cohesive method (VMCM), which is a numerical framework to embed cohesive models into continuum elements, and demonstrating its effectiveness by simulating mixed-mode failure in fiber-reinforced composites.

Since the aim is to present and validate a physically consistent and numerically objective cohesive crack propagation framework which involves elemental enrichment to capture the discontinuous modes associated with crack propagation, it is worthwhile to note that a comparable, but significantly different development, involving nodal enrichment by partition of unity functions, like the extended finite element (XFEM)[11, 18, 19] and[34] also results in objective and physically consistent simulations of crack problems, and the differences and merits of the elemental enrichment over nodal enrichment are highlighted in the concluding section.

This paper is organized as follows: In Section II, the variational multiscale concept of subgrid scale phenomena like cracks is introduced. Then the concept is extended to cracks represented as discontinuous displacement modes and the relevant weak formulation of the problem is derived. This formulation is then cast in a finite element framework in Section III, which presents the multiscale element construction and the resulting discretized equations. The analytical and numerical framework developed until this point is demonstrated through simulation of crack propagation in laminated fiber reinforced composites in Section IV, and by comparison with experimental observations in Section V. Lastly, concluding remarks about the numerical framework and its applicability are provided in Section VI.

II.   Variational Multiscale Formulation

Physically, crack propagation is a process of configurational change by which new surfaces are created. The creation of new surfaces is governed by surface laws, different from the constitutive laws of the continuum. Classically, this process of surface creation is handled by effecting changes in the numerical discretization, involving incremental grid refinement and remeshing. However, changing the grid to reflect the evolving domain boundaries is computationally very expensive. Instead, an alternative view of cracks as displace-

ment discontinuities in the continuum domain is considered here. The concept of discontinuous displacement fields and the resulting singular strains finds its mathematical treatment in the work of[32] on BD(Ω), the space of bounded deformations for which all components of the strain are bounded measures. This idea was used to develop a numerical framework for the problem of strong discontinuities due to strain localization by.[1, 28, 29] The physical process of strain localization involves localized changes in the continuum constitutive response and no new boundaries and surface laws appear, but its numerical treatment introduced the use of the distributional framework and discontinuous basis functions, which was adopted in[13] for embedding micromechanical surface laws into a macroscopic continuum formulation, albeit in a multiscale setting. The presentation in this work follows and extends these multiscale arguments specifically for numerical representation and evolution of cohesive cracks.

As shown in Figure (3), a crack opening can be mathematically represented by a discontinuous displacement field over an uncracked body. It is not difficult to see that this is rigorous and general enough to represent all possible crack geometries in both two and three dimensional solids. However, the following numerical challenges persist:

- Numerical representation of displacement discontinuities using smooth basis approximations introduce an artificial numerical length scale and thus lead to a mesh subjective scheme. On the other hand, usage of discontinuous basis leads to singular strains.

- Topologically, crack surfaces are zero measure sets in the domain volume. Thus stand alone representations of them would require zero volume mesh elements.

In this work, a discontinuous basis is adopted and the necessary distributional arguments will follow. The use of zero volume elements (interface elements, standard cohesive zone elements, etc.) renders the scheme subjective to the numerical discretization, hence is not considered. Instead a variational multiscale setting is introduced where the crack, represented by a displacement discontinuity, is seen as a subgrid fine scale discontinuous field superposed on a coarse scale field.

A.   Multiscale Formulation of Discontinuous Displacement

The weak formulation of the quasi-static elasticity is the point of departure for the multiscale development. Also, the scope of the presentation is limited to the infinitesimal strain theory of elasticity. Starting with the weak form: For $\mathcal{S} \subset BD(\Omega)$ and $\mathcal{V} \subset H^1(\Omega)$, find $u \in \mathcal{S} = \{v| \ v_i = g_i \text{ on } \Gamma_{g_i}\}$, such that $\forall \ w \in \mathcal{V} = \{v| \ v_i = 0 \text{ on } \Gamma_{g_i}\}$,

$$\int_{\Omega} \nabla w : \sigma \ dV = \int_{\Omega} w \ f \ dV + \int_{\Gamma_h} w \ T \ dS \tag{1}$$

where f is the body force, g_i and T are the prescribed boundary displacement and surface traction, respectively. σ is the (Cauchy) stress tensor given by $\sigma = \mathbb{C} : \text{sym}(\nabla u)$, where $\mathbb{C}$ is the fourth-order elasticity tensor.

Scale decompositions of u and w are now introduced. The decompositions are qualified by requiring that the fine scales, u' and w', vanish outside the neighborhood of the crack path, which is contained in Ω' (Figure (4)), which is referred to as the microstructural or fine-scale subdomain

$$u = \underbrace{\overline{u}}_{\text{coarse scale}} + \underbrace{u'}_{\text{fine scale}} \tag{2a}$$

$$w = \underbrace{\overline{w}}_{\text{coarse scale}} + \underbrace{w'}_{\text{fine scale}} \tag{2b}$$

$$\overline{u} \in \overline{\mathcal{S}} = \{v| \ v_i = g_i \text{ on } \Gamma_{g_i}\} \tag{2c}$$

$$\overline{w} \in \overline{\mathcal{V}} = \{v| \ v_i = 0 \text{ on } \Gamma_{g_i}\} \tag{2d}$$

$$u' \in \mathcal{S}' = \{v| \ v = 0 \text{ on } \Omega\backslash\text{int}(\Omega')\} \tag{2e}$$

$$w' \in \mathcal{V}' = \{v| \ v = 0 \text{ on } \Omega\backslash\text{int}(\Omega')\} \tag{2f}$$

where $\mathcal{S} = \bar{\mathcal{S}} \oplus \mathcal{S}'$ and $\mathcal{V} = \bar{\mathcal{V}} \oplus \mathcal{V}'$. Further, $\bar{\mathcal{V}}$ and $\mathcal{V}'$ are chosen to be linearly independent.

In the above domain decomposition, a surface Γ^c is now introduced to represent a crack, as shown in Figure (4). As already noted, the classical jump condition on surface tractions which enforces force equilibrium, requires that stress be a continuous field. Thus $[\![\sigma \cdot n]\!] = 0$ and $T_+^c = T_-^c = T^c$. Now invoking linear independence of $\bar{\mathcal{V}}$ and $\mathcal{V}'$,

$$\int_\Omega \nabla \overline{w} : \sigma \; dV = \int_\Omega \overline{w} \; f \; dV + \int_{\Gamma_h} \overline{w} \; T \; dS \tag{3a}$$

$$\int_{\Omega'} \nabla w' : \sigma \; dV = \int_{\Omega'} w' \; f \; dV \tag{3b}$$

Using integration by parts and standard variational arguments,

$$\int_\Omega \nabla \overline{w} : \sigma \; dV = \int_\Omega \overline{w} f \; dV + \int_{\Gamma_h} \overline{w} \; T \; dS \qquad (\overline{\mathrm{W}}) \tag{4a}$$

$$\int_{\Gamma^c} w' \; \sigma \cdot n \; dS = \int_{\Gamma^c} w' \; T^c \; dS \qquad (\mathrm{W}') \tag{4b}$$

$(\overline{\mathrm{W}})$ is the weak form of the coarse scale problem and (W') is the weak form of the fine scale problem. (W') will be used to eliminate the fine scale field, u', from $(\overline{\mathrm{W}})$.

B. Fine-Scale Field and Micromechanics Embedding

The fine scale weak form, (W'), allows us to embed any traction based micromechanical surface-law, represented by T^c, into the continuum formulation. Specifically, for the problem of crack propagation, T^c is a cohesive surface law, which is determined either experimentally or analytically, and models the load bearing ability of the crack wake region. Restricting our discussion to 2D, it can be expressed as

$$T^c = T_n^c n + T_m^c m \tag{5}$$

where n and m are the unit normal and tangent vectors to the crack face, respectively. T_n^c and T_m^c are the normal and tangential tractions on the crack faces, respectively.

Before discussing the specific functional forms of T_n^c and T_m^c, it will be helpful to briefly digress into a discussion u'. The fine scale field, u', is composed of a continuous field and a discontinuous field,

$$u' = M_{\Gamma^c} [\![u]\!] \; , \qquad \text{where } M_{\Gamma^c} = N - H_{\Gamma^c} \tag{6}$$

here N is a continuous basis function defined on Ω', H_{Γ^c} is a Heaviside function which has its discontinuity on Γ^c, and $[\![u]\!]$ can be written as,

$$[\![u]\!] = \underbrace{[\![u_n]\!]}_{\text{opening}} n + \underbrace{[\![u_m]\!]}_{\text{shear}} m \tag{7}$$

where $[\![u_n]\!]$ and $[\![u_m]\!]$ are scalar values representing the normal and tangential components of $[\![u]\!]$, referred to as the *crack face opening displacement* and *crack face shear displacement*, respectively. Further, in the literature, the crack face opening mechanism is referred to as Mode-I and crack face shear mechanism is referred to as Mode-II. This convention will be followed here onward.

Now, in this work, we consider simple micromechanical surface traction laws given by:

$$T_n^c = T_{n_0}^c - \mathcal{H}_n [\![u_n]\!] \tag{8a}$$
$$T_m^c = T_{m_0}^c - \mathcal{H}_m [\![u_m]\!] \tag{8b}$$

where $T_{n_0}^c$ and $\mathcal{H}_n$ are the Mode-I critical opening traction and Mode-I softening modulus, and $T_{m_0}^c$ and $\mathcal{H}_m$ are the Mode-II critical shear traction and Mode-II softening modulus.

C. Coarse-Scale and Fine-Scale Weak Forms

Now we turn our attention to deriving explicit expressions for $(\overline{W})$ and (W') in terms of the displacement fields. Considering Equations (2a) and (6), the expression for strain and stress are:

$$\varepsilon = \nabla\overline{u} + \nabla N \ [\![u]\!] + \delta_{\Gamma^c} \ n \otimes [\![u]\!] \tag{9a}$$

$$\sigma = \mathbb{C} : (\nabla\overline{u} + \nabla N \ [\![u]\!]) \tag{9b}$$

and as explained earlier, only the regular parts of the strain tensor contribute towards the stress. Substituting this stress expression into $(\overline{W})$ and (W'), we obtain the weak form expressions in term of the displacement fields,

$$\int_{\Omega} \nabla\overline{w} : \mathbb{C} : (\nabla\overline{u} + \nabla N \otimes [\![u]\!]) \ dV = \int_{\Omega} \overline{w}f \ dV + \int_{\Gamma_h} \overline{w} \ T \ dS \tag{10}$$

$$\int_{\Gamma^c} w' \ \mathbb{C} : (\nabla\overline{u} + \nabla N \otimes [\![u]\!]).n \ dS = \int_{\Gamma^c} w' \ T^c \ dS \tag{11}$$

now substituting Equation (5) in Equation (11) and rearranging terms,

$$\int_{\Gamma^c} w' L([\![u]\!]) \ dS = \int_{\Gamma^c} w' F(\overline{u}) \ dS \tag{12}$$

where,

$$L([\![u]\!]) = (\ \mathbb{C} : \nabla N \otimes n + \mathcal{H}_n n \otimes n + \mathcal{H}_m m \otimes m \ )[\![u]\!]$$
$$F(\overline{u}) = T^c_{n_0}n + T^c_{m_0}m - \mathbb{C} : \nabla\overline{u}$$

Using Equation (12), $[\![u]\!]$ can be eliminated from Equation (10), and the resulting coarse scale weak form can be solved for $\overline{u}$. Then one can recover the fine-scale variations, u', over the microstructural domain Ω', using Equations (12) and (6).

III. Finite Element Framework

With the multiscale formulation laid out, and explicit weak form expression derived, we now turn our attention to the numerical implementation. Here, the multiscale methodology is cast into a finite element formulation and the necessary numerical framework, referred to as the Variational Multiscale Cohesive Method (VMCM), is developed. First, the necessary discontinuous shape functions are presented and then the finite dimensional weak formulation and dicretized equations are developed.

A. Multiscale Element Construction

The reparametrization of the fine scale discontinuous displacement field introduced in Equation (6) is now reproduced for linear triangular elements, and the presentation follows from the discontinuous shape function's discussion in.[1,12]

1. Shape Functions

We begin with the multiscale basis function expression,

$$M_{\Gamma^c} = N - H_{\Gamma^c} \tag{13}$$

where N is a continuous basis function defined on Ω' and H_{Γ^c} is a Heaviside function which has its discontinuity on Γ^c. Thus, M_{Γ^c} is hereupon considered as a composite shape function constructed by superposing a Heaviside function on a linear shape function, ensuring that $M_{\Gamma^c} = 0$ on $\Omega\backslash\text{int}(\Omega')$. This construction is depicted in Figure (5) for 1D and Figure (6) for 2D. A detailed construction is now presented for the constant strain triangle element.

American Institute of Aeronautics and Astronautics

As shown in Figure (7), there are two possible constructions for triangle elements depending on the relative orientation of the normal to the crack path, n, with respect to the outward normal of the edge not intersected by the crack, n^i. For each of these cases, N, H_{Γ^c} and ∇M_{Γ^c} are given by

Case-I: $n.n^i < 0$ (Figure (7a))

$$N(x) = 1 - \frac{x - x^i}{h^i}.n^i \tag{14}$$

$$H_{\Gamma^c}(x) = \begin{cases} 0 : |(x - x^\Gamma).n| \leq 0 \\ 1 : |(x - x^\Gamma).n| > 0 \end{cases} \tag{15}$$

$$\nabla M_{\Gamma^c}(x) = -\frac{n^i}{h^i} - \delta_{\Gamma^c}\, n \tag{16}$$

Case-II: $n.n^i \geq 0$ (Figure (7b))

$$N(x) = \frac{x - x^i}{h^i}.n^i \tag{17}$$

$$H_{\Gamma^c}(x) = \begin{cases} 0 : |(x - x^\Gamma).n| \leq 0 \\ 1 : |(x - x^\Gamma).n| > 0 \end{cases} \tag{18}$$

$$\nabla M_{\Gamma^c}(x) = \frac{n^i}{h^i} - \delta_{\Gamma^c}\, n \tag{19}$$

As can be seen from the above description, the multiscale shape function construction is more involved than traditional shape functions. In a numerical implementation, only ∇M_{Γ^c} enters the system of equations through the expression for $\nabla u'$, which in matrix form is given by

$$\nabla u' = \nabla M_{\Gamma^c}\, [\![\boldsymbol{u}]\!] \tag{20}$$

where,

$$[\![\boldsymbol{u}]\!] = \begin{bmatrix} [\![u]\!]_x \\ [\![u]\!]_y \end{bmatrix}$$

$$\nabla M_{\Gamma^c} = \frac{1}{h^i} \underbrace{\begin{bmatrix} n_x^i & 0 \\ 0 & n_y^i \\ n_y^i & n_x^i \end{bmatrix}}_{\boldsymbol{G}} - \delta_{\Gamma^c} \underbrace{\begin{bmatrix} n_x & 0 \\ 0 & n_y \\ n_y & n_x \end{bmatrix}}_{\boldsymbol{H}}$$

$\boldsymbol{G}$ and $\boldsymbol{H}$ are the matrix representation of n^i and n, respectively.

2. Numerical Quadrature

The weak form of the coarse scale and fine scale problems, given by Equations (10) and (12), respectively, involve different domains of integration. The coarse scale weak form, taken element wise, is a volume integral over the elemental volume and thus the quadrature rules used to evaluate the integral is the conventional triangle quadrature scheme. However, the fine scale weak form, taken element wise, is a surface integral over the crack path, and needs special attention.

Consider Figure (8) which depicts a constant crack opening displacement, $[\![u]\!]$, in linear triangles. For this case, since the stress is also constant over the element, a one point quadrature rule is sufficient for the fine scale weak form. This reduces Equation (12) to $\sigma \cdot n = T^c$ which can be evaluated at any point along the crack path within the element.

B.   Finite Dimensional Weak Forms and Discretized Equations

In the finite dimensional setting, the problem domain is divided into non overlapping elements such that $\Omega = \bigcup_1^{nel} \Omega_e^h$, where nel is the number of elements. In this presentation linear triangle elements are considered, and thus the integration scheme depicted in Figure (9a) will be sufficient. Introducing the approximate interpolations to the coarse-scale displacement and variation,

$$\bar{u}_e^h(\xi, \eta) = \sum_{A=1}^{3} N^A(\xi, \eta) d^A \tag{21a}$$

$$\bar{w}_e^h(\xi, \eta) = \sum_{A=1}^{3} N^A(\xi, \eta) c_e^A \tag{21b}$$

where (ξ, η) are the iso-parametric coordinates, d^A and c_e^A are the nodal values of the finite dimensional coarse-scale displacement, $\bar{u}^h$, and finite dimensional coarse-scale variation, $\bar{w}^h$, respectively. $N^A(\xi, \eta)$ is the Lagrangian shape function at node A with the usual compact support, $N^A(\xi_B, \eta_B) = \delta_B^A$. Adopting matrix notation,

$$\bar{u} = \boldsymbol{N}\boldsymbol{d} \qquad \text{and} \qquad \bar{w} = \boldsymbol{N}\boldsymbol{c} \tag{22}$$

$$\nabla\bar{u} = \boldsymbol{B}\boldsymbol{d} \qquad \text{and} \qquad \nabla\bar{w} = \boldsymbol{B}\boldsymbol{c} \tag{23}$$

where $\boldsymbol{B}$ is the standard matrix form of the shape function gradients. Similarly, the vector representation of the Equations (9a), (9b) for strain and stress are

$$\varepsilon = \boldsymbol{B}\boldsymbol{d} + (\boldsymbol{G} - \delta_{\Gamma^c}\boldsymbol{H})\, [\![\boldsymbol{u}]\!] \tag{24a}$$

$$\sigma = \mathbb{C} : (\boldsymbol{B}\boldsymbol{d} + \boldsymbol{G}\, [\![\boldsymbol{u}]\!]) \tag{24b}$$

Substituting the above expressions into Equations (10) and (11), the respective finite dimensional equations are given by

$$\int_\Omega \boldsymbol{B}^T \mathbb{C} : (\boldsymbol{B}\boldsymbol{d} + \boldsymbol{G}\, [\![\boldsymbol{u}]\!])\, dV = \int_\Omega \boldsymbol{N} f\, dV + \int_{\Gamma_h} \boldsymbol{N}\, T\, dS \tag{25a}$$

$$\boldsymbol{H}^T \mathbb{C} : (\boldsymbol{B}\boldsymbol{d} + \boldsymbol{G}\, [\![\boldsymbol{u}]\!]) = \boldsymbol{T^c} \tag{25b}$$

where the fine-scale weak form is reduced to $\sigma \cdot n = T^c$, as for linear triangles both σ and $[\![\boldsymbol{u}]\!]$ (and hence $\boldsymbol{T^c}$) are constant over the element. To suit an iterative solution procedure, the above equations are expressed as coarse-scale and fine-scale residuals,

$$\bar{r} = \int_\Omega \boldsymbol{B}^T \mathbb{C} : (\boldsymbol{B}\boldsymbol{d} + \boldsymbol{G}\, [\![\boldsymbol{u}]\!])\, dV - \int_\Omega \boldsymbol{N} f\, dV - \int_{\Gamma_h} \boldsymbol{N}\, T\, dS \tag{26a}$$

$$r' = \boldsymbol{H}^T \mathbb{C} : (\boldsymbol{B}\boldsymbol{d} + \boldsymbol{G}\, [\![\boldsymbol{u}]\!]) - \boldsymbol{T^c} \tag{26b}$$

Linearizing the above residuals about $\boldsymbol{d}$ and $[\![\boldsymbol{u}]\!]$ and rearranging terms, we obtain the following system of equations in $(\delta\boldsymbol{d}, \delta[\![\boldsymbol{u}]\!])$,

$$\begin{bmatrix} \boldsymbol{K}_{\bar{u}\bar{u}} & \boldsymbol{K}_{\bar{u}u'} \\ \boldsymbol{K}_{u'\bar{u}} & \boldsymbol{K}_{u'u'} \end{bmatrix} \begin{bmatrix} \delta\boldsymbol{d} \\ \delta[\![\boldsymbol{u}]\!] \end{bmatrix} = \begin{bmatrix} -\bar{r} \\ -r' \end{bmatrix} \tag{27}$$

where,

$$\boldsymbol{K}_{\bar{u}\bar{u}} = \int_\Omega \boldsymbol{B}^T \mathbb{C} \boldsymbol{B}\, dV \tag{28a}$$

$$\boldsymbol{K}_{\bar{u}u'} = \int_\Omega \boldsymbol{B}^T \mathbb{C} \boldsymbol{G}\, dV \tag{28b}$$

$$\boldsymbol{K}_{u'\bar{u}} = \boldsymbol{H}^T \mathbb{C} \boldsymbol{B} \tag{28c}$$

$$\boldsymbol{K}_{u'u'} = \boldsymbol{H}^T \mathbb{C} \boldsymbol{G} + \mathcal{H}_n \boldsymbol{n} \otimes \boldsymbol{n} + \mathcal{H}_m \boldsymbol{m} \otimes \boldsymbol{m} \tag{28d}$$

American Institute of Aeronautics and Astronautics

IV. Numerical Simulations

With the multiscale formulation and the finite element implementation developed, this section presents numerical simulations of some benchmark problems to demonstrate the effectiveness and applicability of the multiscale framework for cohesive crack propagation. All simulations are in 2D and assume plane strain conditions. Further, as indicated in earlier section, a crack tracking algorithm is required as part of the iterative process to evolve the crack from one element to another. Such an algorithm should be based on a physically relevant crack direction criterion, and may be material and microstructure subjective. In this work, it is assumed that the crack propagates along a path that renders the shear stress to be zero. This amounts to assuming that the crack is locally governed by a Mode-I criterion. However, the direction criterion places no limitation on the multiscale formulation and depending on the material micromechanics, any relevant direction criterion can be chosen.

It is also pointed out that apparent distortion of the elements may be seen as contradicting the small strain assumption of linear elasticity and also potentially result in singular Jacobians for those elements. This is not the case as:

- The regular part of the strain is always small, and the singular components which lead to this observed element distortion do not contribute to the stress-strain constitutive relation (Section (A)).

- Since the implementation is in the reference configuration, the element distortion has no effect on the elemental Jacobian determinant.

To remove this potential confusion, the crack path elements are removed from the plots, except in Section (A) where the discussion is primarily on the element level.

All the simulations were carried out using an in-house, C++ based, variational multiscale cohesive method (VMCM) finite element code developed by the author. A standard Newton-Raphson scheme was used for solving the system of non-linear equations, based on a direct solution procedure using the SuperLU library.[10]

A. Mesh Objectivity Demonstration

As stated previously, eliminating pathological mesh dependence of crack propagation simulations is one of the primary motivations for the development of the multiscale framework, and this section seeks to demonstrate the mesh objectivity of this implementation. The results presented in this section focus on the dependence of the global load-displacement response and the crack path, the two most important metrics from a structural viewpoint, on the mesh density.

1. Straight Crack Propagation

Consider the problem of a cohesive tension block under uniaxial tension, as shown in Figure (11). Shown are the problem schematic, resulting crack paths for meshes whose density varies over two orders of magnitude, and the corresponding global load-displacement response. It should be sufficiently clear from this result that the traditional pathological mesh dependence is completely absent for the case of a straight crack path. However, this physical problem involves no crack turning, so the sensitivity of the crack path is not manifested here. A more complex problem involving curved crack propagation is presented in the following subsection.

The load-displacement response in Figure (11 C) is physically relevant, as it indicates that the strain energy release rate, G, and the surface energy density, γ' are mesh independent, because the area under the curve is equal to the energy dissipated due to surface creation.

2. Curved Crack Propagation

Figure (12) shows the response of a standard Single Edge Notch Three-Point Bend (SETB) specimen under eccentric loading conditions. Due to the unsymmetrical loading, the crack deviates from its straight path and approaches the loading point as this is the contour of the maximum normal tractions, and the load-displacement and crack path is objectively simulated across all the mesh densities considered. However, at

American Institute of Aeronautics and Astronautics

first glance, the small variation in the load-displacement response and crack path may suggest mesh sensitivity. This is expected, as even in the absence of cracks, the resolution of the high stress gradients does depend to a small degree on the element dimension, and this naturally effects the crack direction determination and consequently the load-displacement response. Thus, these small variations are not pathological, as can be seen from Figure (12 C), but an artifact of the numerical discretization.

B. Mixed Mode Crack Propagation

Mixed-mode refers to the condition where the crack face is subjected to both in plane and out of plane tractions. In 2D, this means that the crack face is under the influence of mode-II shear tractions in addition to the Mode-I opening tractions. Crack propagation involving non-straight paths is often mixed-mode and so their will be two cohesive traction-separation relations corresponding to normal-opening and shear-slipping modes. This section demonstrates the mixed-mode fracture simulation capability of the multiscale implementation. As stated earlier, the crack path elements are removed and for better visualization only the field contours are shown, without the underlying mesh.

Figure (14) shows snapshots of crack propagation in a symmetrically loaded Compact Tension (CTS) specimen. Although the mixed-mode scheme is active, the symmetry in the specimen and loading result in near straight crack propagation with very little crack face shear. However, the opening stress contours provide insights into the load bearing ability of materials with large process zone sizes. As seen in the evolving contour plots, the majority of the stress concentration is in the crack wake and this provides resistance to crack growth. This increased resistance to crack growth can also be implied from the corresponding load-displacement response which is flat indicating the increased fracture toughness of this material. The crack face bridging, as evident from the stress contours, gradually increases in size, then approaches a steady state value before shortening as the crack approaches the specimen boundary where the compressive stress is significant due to bending. More detailed analysis of the bridging zone evolution will be presented in the next chapter.

Figure (13) shows mixed-mode curved crack propagation in an eccentrically loaded SETB specimen where the crack approaches the loading point along the contour of the maximum normal tractions. Similarly, Figure (16) shows crack propagation in a rectangular specimen with a fully constrained left end and a displacement loading at the lower right corner. Also, it is experimentally observed that the crack propagation in laminated fiber reinforced composite materials is predominantly along the fiber layup direction, so the effect of restricting the crack propagation direction in VMCM simulations is shown in Figure (17), where the crack path is restricted to the -45/0/+45/+90 fiber layup directions.

C. Interacting and Multiple Cracks

In this subsection, complexity due to multiple cracks, interactions between cracks and interaction with structural inclusions is addressed. It is stressed that the multiscale formulation has no restriction on the number of possible cracks in a domain or on their interaction, but possible complexity may arise due to modifications required to the traction-separation relations to produce physically consistent simulations.

Consider the standard Double Edge Notch Tension (DENT) specimen crack propagation simulation in Figure (15). As expected two cracks start from notches on either side and approach each other, and the opening stress contours show their interactions. Initially, either crack grows independently, but as they get closer they interact through the long range terms of the asymptotic expansion of the crack tip stress. However, due to the small offset in their crack paths, induced due to the numerical discretization, they pass each other. But eventually the crack paths intersect and one branch of the combined crack becomes predominant while the other branch relaxes. This problem also serves as an example of how, an otherwise complex crack interaction, can be clearly understood through the numerical implementation.

V.   Experimental Validation

The numerical implementation needs a traction-separation relation as input, in addition to the material properties listed in Table VI, to simulate crack propagation. Here we assume a linear traction-separation

relation which is characterized by the peak traction value T_{n_0} and the fracture toughness R_{avg}. T_{n_0} is a fixed value for all the specimen geometries, and is obtained from standard double edge notch tension (DENT) specimen experiments. It is noted that, traditional cohesive zone models employ a traction law that starts with a zero traction and zero opening, whereas, in the VMCM, the transition from a continuum to a non-continuum (cracking) takes place at a finite traction (Figure 2). The ramifications of this aspect have been discussed in the literature.[15, 31]

The simulations are conducted with the experimentally measured R_{avg} values given in Table 2, and the results are plotted in Figure 18 for a symmetrically loaded specimen, and Figure 19 for eccentrically loaded specimen which has mixed mode curved crack growth. Further details of the experiments are provided in.[25]

As seen from Figure 18, the multiscale simulations accurately reproduce the macroscopic response of the SETB specimens when appropriate R_{avg} values are used as input.[a] This demonstrates that: (1) The multiscale methodology has the ability to numerically simulate progressive damage propagation, and the mechanics of bridged crack evolution. (2) In spite of a multitude of failure mechanisms operating simultaneously, leading to a very complex evolution of fracture resistance, the single valued estimate, R_{avg}, of the fracture resistance is appropriate for numerical simulations, at least in this class of materials.[b]

VI. Conclusions

In this paper, the variational multiscale cohesive method (VMCM),[23–26] has been extended to simulate mixed-mode, in-plane crack propagation in laminated fiber reinforced composite laminates, as a part of ICE. Experimental results that correspond to single edge notch three point-bend (SETB) specimens have been used as the basis for validating the proposed methodology. Numerical simulations corresponding to several other configurations of crack growth, where the crack path is not known a-priori have been presented. The subtle, but nevertheless important, distinction between the elemental enrichment based multiscale interpolation (adopted in VMCM) and other nodal enrichment based discontinuity interpolation schemes has been depicted in Figure (20). Though both methods represent the displacement discontinuity as a Heaviside function, the advantage of the VMCM approach is the *local-to-element* nature of the fine scale field. From a numerical standpoint this implies that the additional degrees of freedom needed to represent $[\![u]\!]$ can be separated locally through static condensation, and thereby does not contribute to the global solution vector. This also ensures that the sparsity pattern of the global stiffness matrix is unaltered. In contrast, nodal enrichment methods add extra nodal degrees of freedom to represent the enhanced displacement discontinuity modes, thereby altering the global solution vector and stiffness matrix structure with crack propagation. While a more detailed comparative study of the computational complexity, numerical stability and consistency are a topic for future work, interested readers are pointed to a related study[20] between the elemental enrichment method, from which the VMCM method inherits its interpolation characteristics, and the nodal enrichment based extended finite element (X-FEM) method.

Acknowledgments

References

[1] Armero, F. & Garikipati, K., *"An analysis of strong discontinuities in multiplicative finite strain plasticity and their relation with the numerical simulation of strain localization in solids"*, International Journal of Solids and Structures 33 (20-22), 2863 – 2885, 1996,

---

[a] The small pre-peak stiffness difference in the experimental curves of some specimens is due to some amount of material crushing occurring at the loading points, and the post-peak variations are an artifact of the stochastic nature of failure in these materials.

[b] Even though the linear traction separation law simplifies a set of complex failure mechanisms, the dissipated energy is well-represented. This quantity appears to control the fit with experimental $P\Delta$ curves.

[2]Aveston, J., Cooper, G. A. & Kelly, A., *"The properties of fiber composites"*. Conference Proceedings, National Physical Laboratory (IPC Science and Technology Press Ltd), 1971.

[3]Aveston, J. & Kelly, A., *"Theory of multiple fracture of fibrous composites"*. Journal of Materials Science 8, 352–362, 1973.

[4]Bazant, Z., *"Mechanics of distributed cracking"*, Applied Mechanics Reviews, 39, 675–705. 1986.

[5]Camacho, G. T. & Ortiz, M., *"Computational modeling of impact damage in brittle materials"*, International Journal of Solids and Structures 33, 2899–2938, 1996.

[6]Chadwick, P., *"Continuum Mechanics Concise Theory and Problems"*, Dover Publications, 1999.

[7]Cooper, G. A.,*"The fracture toughness of composites reinforced with weakened fibers"*, Journal of Materials Science 5, 645–654, 1970.

[8]Cox, B. N., *"Extrinsic factors in the mechanics of bridged cracks"*, Acta metallurgica et materialia 39, 1189–1201, 1991.

[9]Crisfield, M. A. & Wills, J., *"Solution strategies and softening materials"*, Computer Methods in Applied Mechanics and Engineering 66 (3), 267 – 289, 1988.

[10]Demmel, J. W., Eisenstat, S. C., Gilbert, J. R., Li, X. S. & Liu, J. W. H.,*"A supernodal approach to sparse partial pivoting"*, SIAM J. Matrix Analysis and Applications 20 (3), 720–755, 1999.

[11]Dolbow, J., Mos, N. & Belytschko, T., *"An extended finite element method for modeling crack growth with frictional contact"*, Computer Methods in Applied Mechanics and Engineering 190 (51-52), 6825 – 6846, 2001.

[12]Garikipati, K., *"On strong discontinuities in inelastic solids and their numerical simulation"*, Ph.D. Thesis, Stanford University, 1996.

[13]Garikipati, K., *"A variational multiscale method to embed micromechanical surface laws in the macromechanical continuum formulation"*, Computer Modeling in Engineering and Sciences 3 (2), 175 – 184, 2002.

[14]Heinrich, C., Aldridge, M., Wineman, A.S., Kieffer, J. & Waas, A.M., *"Integrated computational materials science and engineering of textile polymer composites"*, Proceedings of the 52nd AIAA/ASME/ASCE/AHS/ASC Structures, Structural Dynamics, and Materials Conference, Denver, Colorado, USA, 2011.

[15]Jin, Z.-H. & Sun, C., *"Cohesive zone modeling of interface fracture in elastic bi-materials"*, Engineering Fracture Mechanics 72 (12), 1805 – 1817, international Conference of Heterogeous Material Mechanics, Chongqing University and Yangtze River/Three Gorges, China, June 21-26, 2004.

[16]Kellogg, O. D., *"Foundations of potential theory"*, Dover Publications, 1953.

[17]Larsson, R., Runesson, K. & Ottosen, N. S., *"Discontinuous displacement approximation for capturing plastic localization"*, International Journal for Numerical Methods in Engineering 36, 20872105, 1993.

[18]Moes, N. & Belytschko, T., *"Extended finite element method for cohesive crack growth"*, Engineering Fracture Mechanics 69 (7), 813 – 833, 2002.

[19]Moes, N., Dolbow, J. & Belytschko, T., *"A finite element method for crack growth without remeshing"*, International Journal for Numerical Methods in Engineering 46, 131 – 150, 1999.

[20]Oliver, J., Huespe, A. & Snchez, P., *"A comparative study on finite elements for capturing strong discontinuities: E-fem vs X-fem"*, Computer Methods in Applied Mechanics and Engineering 195 (37-40), 4732 – 4752, John H. Argyris Memorial Issue. Part I, 2006.

[21]Pietruszczak, S. T. & Mroz, Z., *"Finite element analysis of deformation of strain softening materials"*. International Journal for Numerical Methods in Engineering 17, 327–334, 1981.

[22]Ramakrishnan, N., Okada, H. & Atluri, S. N., *"On shear band formation: II. Simulation using finite element method"*, International Journal of Plasticity 10 (5), 521 – 534, 1994.

[23]Rudraraju, S. S., *"On the theory and numerical simulation of cohesive crack propagation with application to fiber-reinforced composites"*, Ph.D. Thesis, University of Michigan Ann Arbor, 2011.

[24]Rudraraju, S. S., Salvi, A., Garikipati, K. & Waas, A. M., *"A multiscale crack path predicting computational method for laminated fiber reinforced composites"*, Proceedings of the 49th AIAA/ASME/ASCE/AHS/ASC Structures, Structural Dynamics, and Materials Conference, Schaumburg, Illinois, USA, 2008.

[25]Rudraraju, S. S., Salvi, A., Garikipati, K. & Waas, A. M, *"In-plane fracture of laminated fiber reinforced composites with varying fracture resistance: Experimental observations and numerical crack propagation simulations"*, International Journal of Solids and Structures 47 (7-8), 901 – 911, 2010.

[26]Rudraraju, S. S., Salvi, A., Garikipati, K. & Waas, A. M, *"Mixed mode in-plane fracture analysis of laminated fiber reinforced composites using the variational multiscale cohesive method"*. Proceedings of the 51st AIAA/ASME/ASCE/AHS/ASC Structures, Structural Dynamics, and Materials Conference, Orlando, Florida, USA, 2010.

[27]Schellekens, J. C. J. & DeBorst, R., *"On the numerical integration of interface elements"*, International Journal for Numerical Methods in Engineering 36, 43–66, 1993.

[28]Simo, J. C. & Oliver, J., *"A new approach to the analysis and simulation of strain softening in solids"*, Fracture and Damage in Quasibrittle Structures, 1994.

[29]Simo, J. C., Oliver, J. & Armero, F, *"An analysis of strong discontinuities induced by strain-softening in rate-independent inelastic solids"*, Computational Mechanics 12, 277–296, 1993.

[30]Song, S. & Waas, A, *"A nonlinear elastic foundation model for crack growth in laminates"*, J. Composites Engineering 3, 945–959, 1993.

[31]Sun, C. & Jin, Z.-H, *"Modeling of composite fracture using cohesive zone and bridging models"*, Composites Science and Technology 66 (10), 1297 – 1302, 2006.

[32]Temam, R. & Strang, G, *"Functions of bounded deformation"*, Archive for Rational Mechanics and Analysis 75, 7–21, 1980.

[33]Ungsuwarungsri, T. & Knauss, W. G, *"The role of damage-softened material behavior in the fracture of composites and adhesives"*, International Journal of Fracture 35, 221–241, 1987.

[34]Wells, G. N. & Sluys, L. J., *"A new method for modelling cohesive cracks using finite elements"*, International Journal for Numerical Methods in Engineering 50, 2667 – 2682, 2001.

[35]Xie, D., Salvi, A., Sun, C., Waas, A. M. & Caliskan, A. *"Discrete cohesive zone model to simulate static fracture in 2-d triaxially braided carbon fiber composites"*, Journal Composite Materials 40, 1–22, 2006.

[36]Xie, D. & Waas, A. M, *"Discrete cohesive zone model for mixed-mode fracture using finite element analysis"*, Engineering Fracture Mechanics 73, 1783–1796, 2006.

[37]Xu, X. P. & Needleman, A, *"Numerical simulation of fast crack growth in brittle solids"*, Journal of the Mechanics and Physics of Solids 42, 1397–1434, 1994.
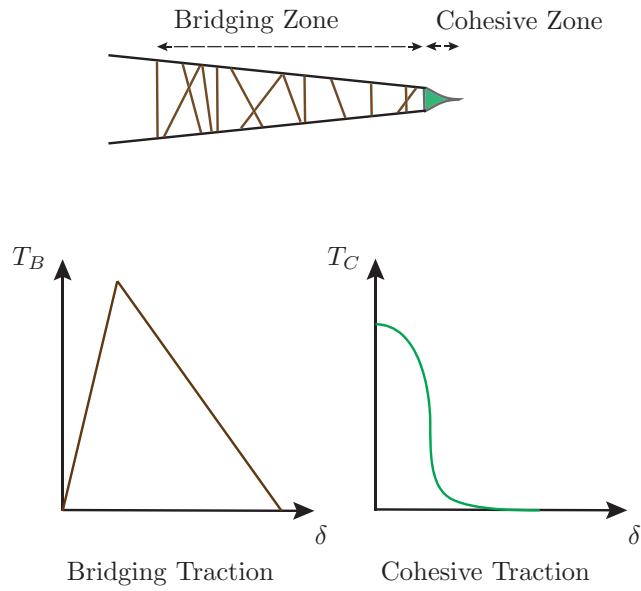
Figure 1. Schematics of possible bridging traction-separation and cohesive traction-separation relations.
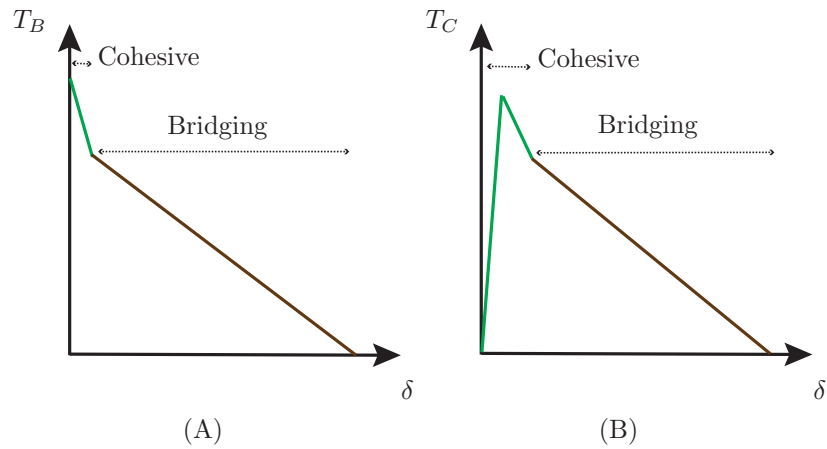
Figure 2. Schematic of possible mixed cohesive-bridging traction-separation relations (A) Physically consistent as cohesive relation begins at finite traction, (B) Physically inconsistent as cohesive relation begins at zero traction.
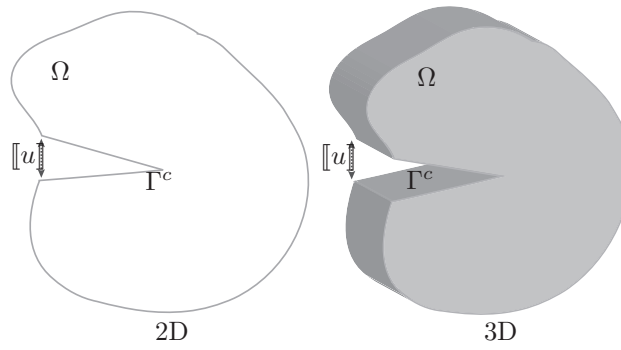
Figure 3. Representation of crack as a displacement discontinuity. $[\![u]\!]$ **is the magnitude of the displacement discontinuity which physically represents the magnitude of the crack opening and** Γ^c **is the crack surface.**
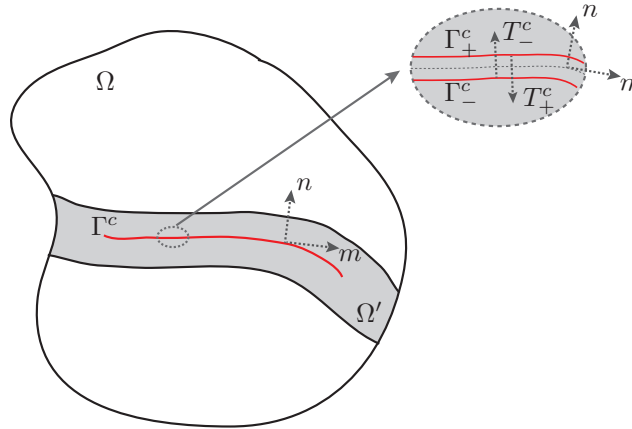
Figure 4. The microstructural domain, Ω'**, and the crack surface,** Γ^c**. Shown in the inset are the crack orientation vectors and the crack surface tractions.** Γ^c_+**,** Γ^c_- **are the top and bottom crack surfaces and** T^c_+**,** T^c_- **are tractions on these surfaces.**
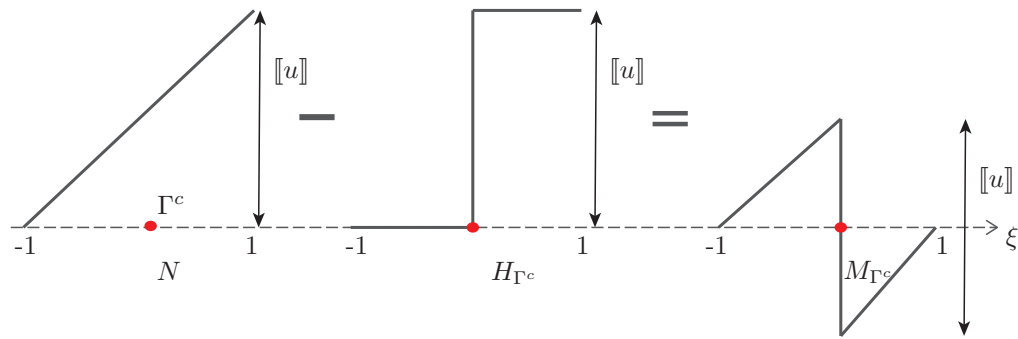
Figure 5. Construction of the discontinuous multiscale shape function in 1D.

Table 1. Lamina and laminate properties of carbon fiber/epoxy $[-45/0/+45/90]_{6s}$ **laminated fiber reinforced composite.**

Laminate	Lamina
E_{xx}: 51.5 GPa	E_{11}: 141 GPa
E_{yy}: 51.5 GPa	E_{22}: 6.7 GPa
G_{xy}: 19.4 GPa	G_{12}: 3.2 GPa
ν_{xy}: 0.32	ν_{12}: 0.33

(a)

(b)
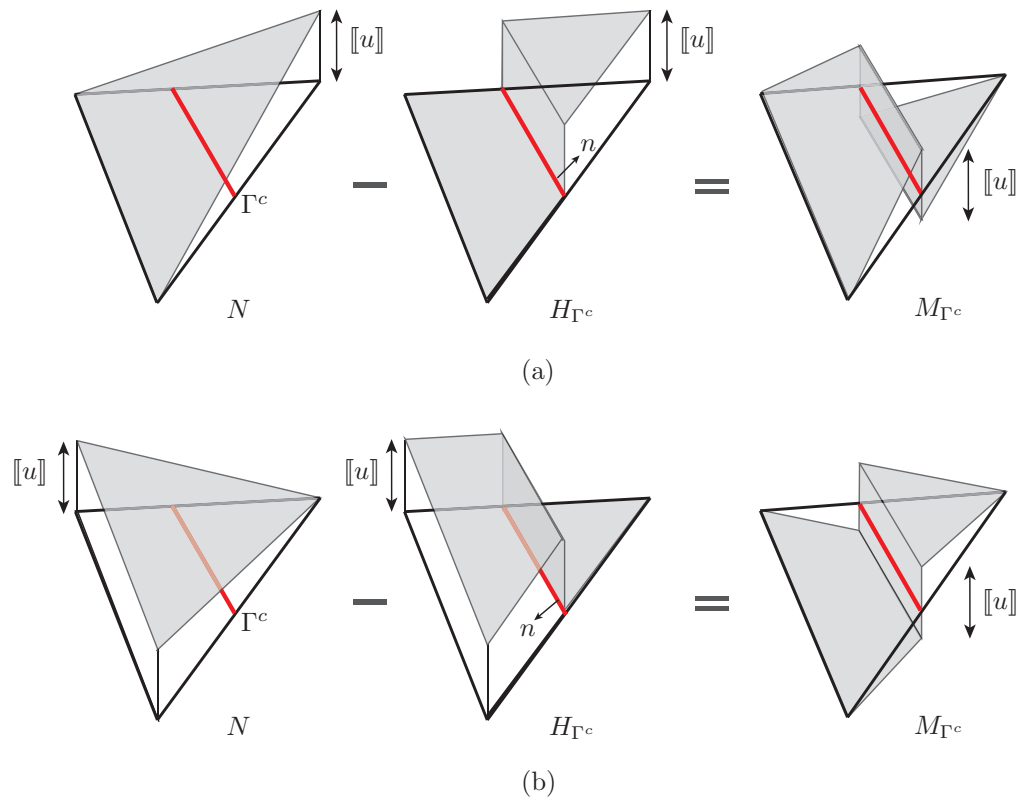
Figure 6. Possible constructions of the discontinuous multiscale shape function in 2D. n **is the normal to the crack path, in the direction of the desired jump in displacement.**

Table 2. Scaling observed in the SETB specimen experiments.

Size	Geometry scaling (Figure 10)	Peak load P/P^*	Load point displacement Δ/Δ^*	Fracture resistance R_{avg}/R_{avg}^*
1	1	0.27	0.1	1.08
2	1.5	0.4	0.15	1.23
3	2	0.6	0.2	1.84
4	3	0.81	0.28	2.46
5	4	1.0	0.37	2.58
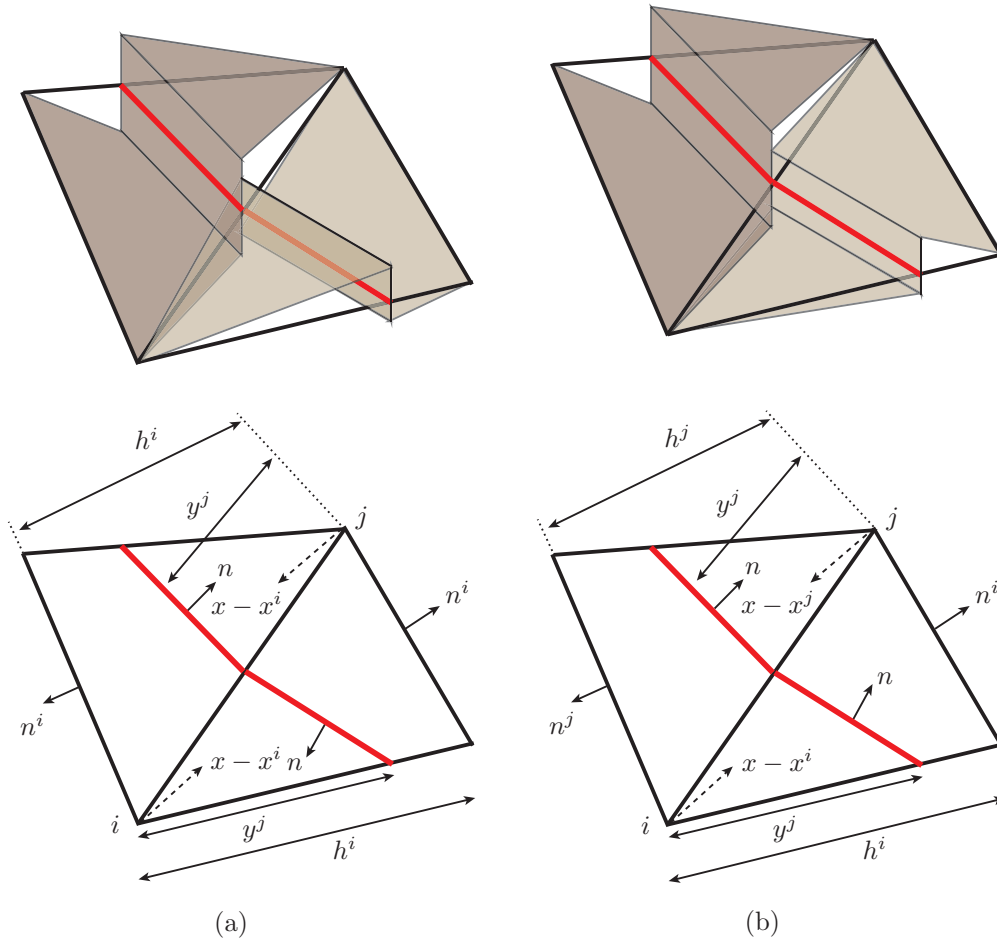
Figure 7. Possible constructions for triangle elements depending on the relative orientation of the normal to the crack path, n, with respect to the outward normal of the edge not intersected by the crack, n^i.
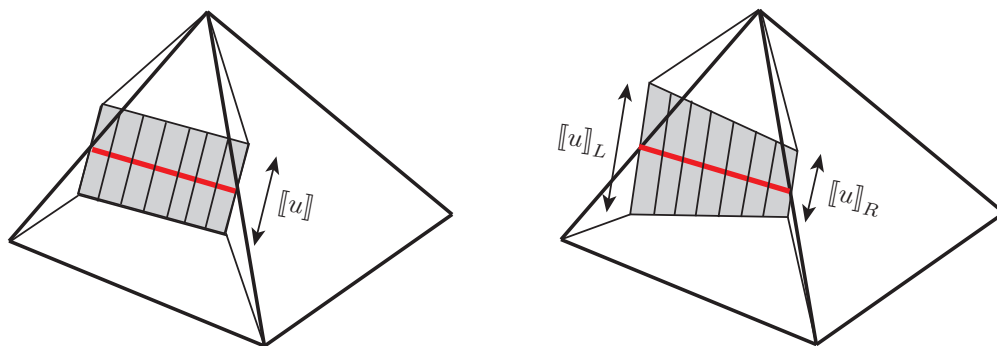
Figure 8. Elemental values of the displacement discontinuity, $[\![u]\!]$, which physically represents the crack opening. (a) Constant $[\![u]\!]$ in each element, (b) Linearly varying $[\![u]\!]$ with $[\![u]\!]_L$ on the left edge and $[\![u]\!]_R$ on the right edge, leading to inter-element continuity along Γ.
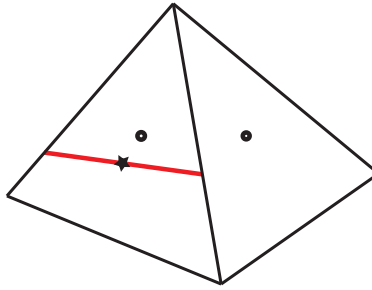
Figure 9. Schematic of quadrature points for coarse-scale and fine-scale problem over a linear triangle element
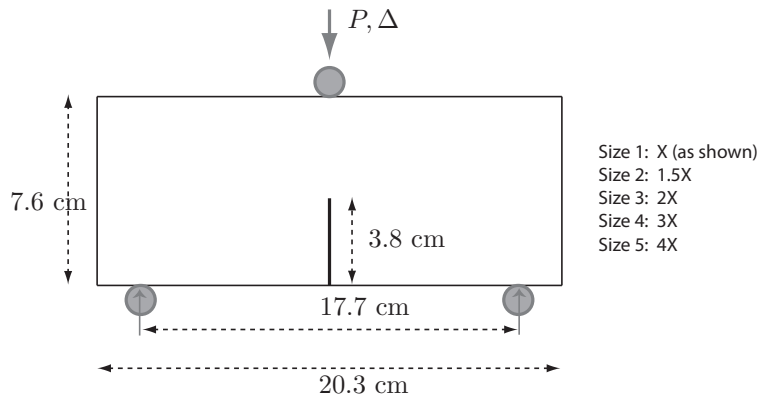
Figure 10. Single Edge Notch Bending(SETB) specimen configuration used for validating VMCM simulation results. Size 1 has the dimensions shown in figure, other sizes are scaled versions of this base size. All specimens have a nominal thickness of 6.35mm.

American Institute of Aeronautics and Astronautics
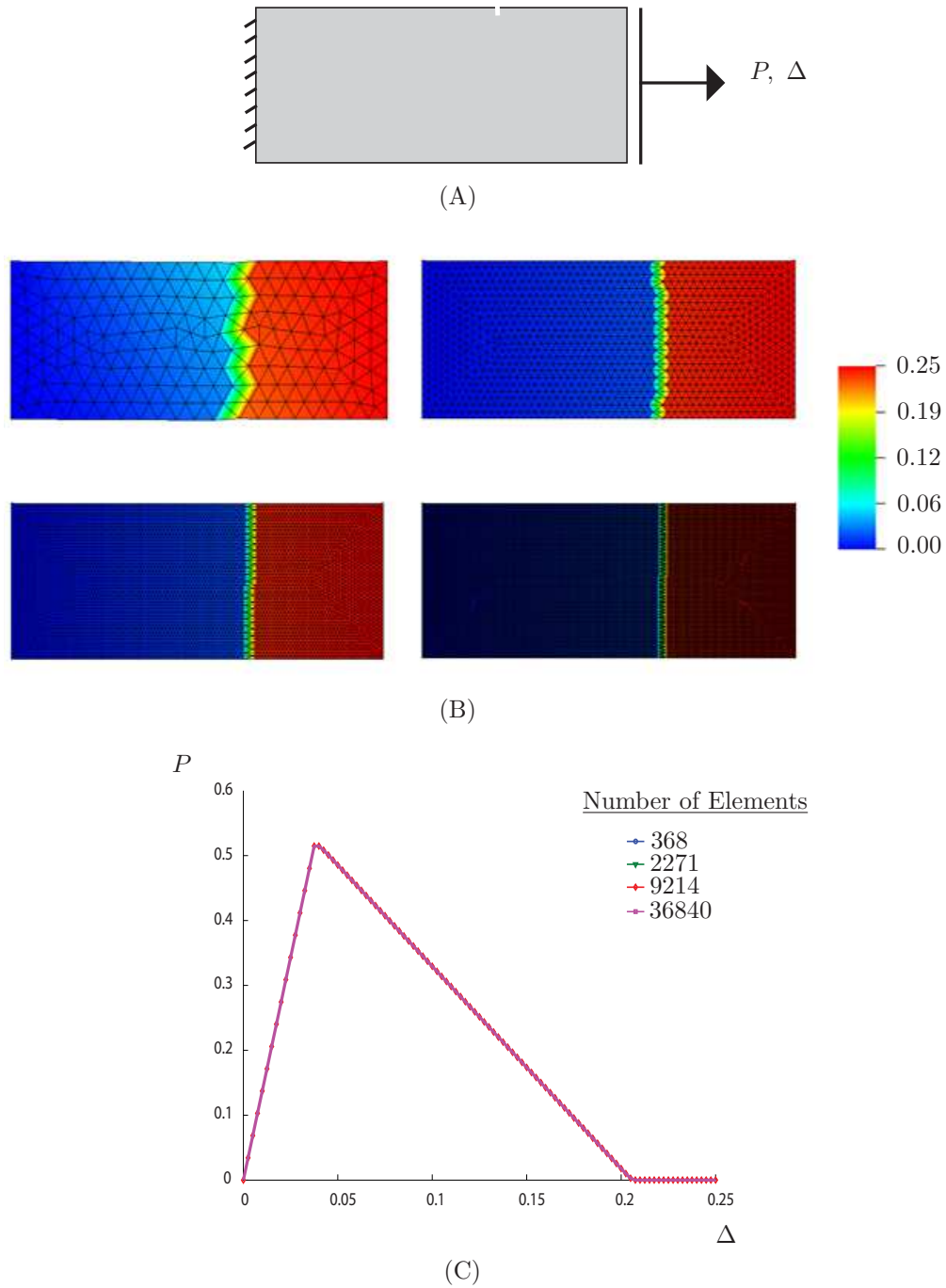
Figure 11. Mesh objectivity for straight crack propagation. (A) Rectangular cohesive material under uni-axial tension, (B) Displacement magnitude contours for different mesh densities, (C) Corresponding load-displacement response. The P and Δ values have been normalized with fixed reference values.
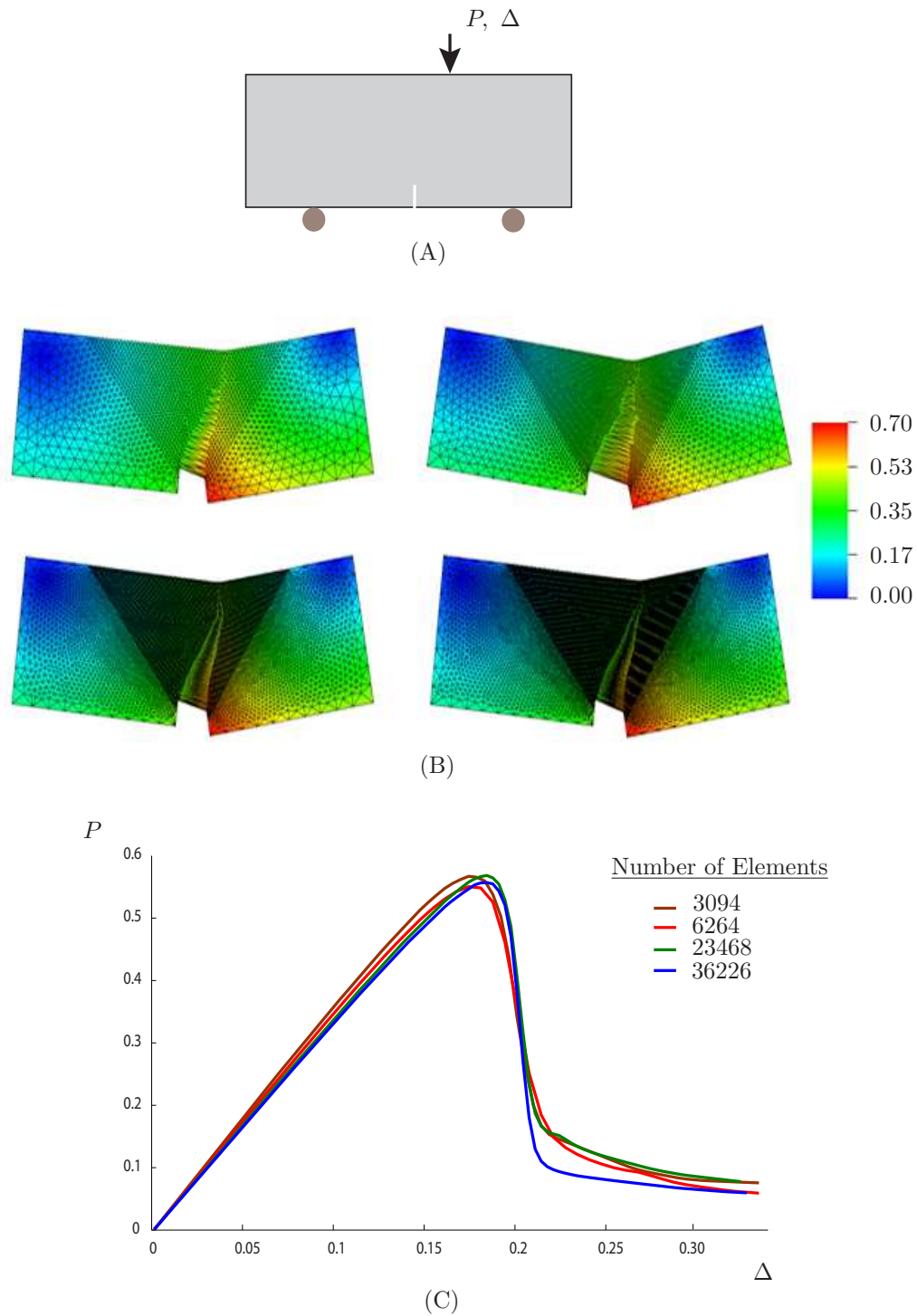
**Figure 12. Mesh objectivity for curved crack propagation.** (A) Eccentrically loaded SETB specimen, (B) Displacement magnitude contours for different mesh densities, (C) Corresponding load-displacement response. The P and Δ values have been normalized with fixed reference values.

American Institute of Aeronautics and Astronautics
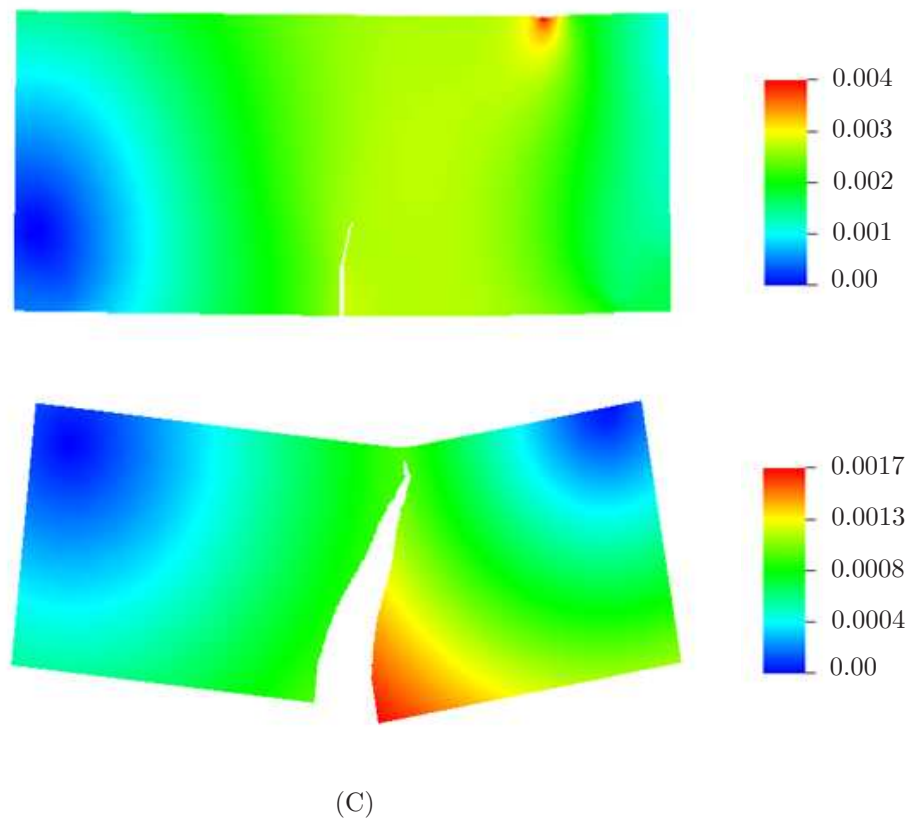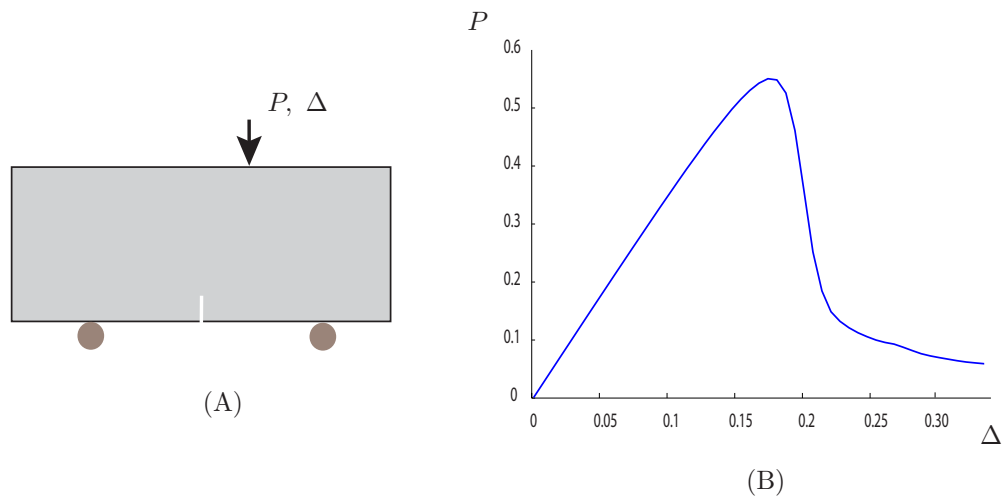
Figure 13. Mixed-mode crack propagation in an eccentrically loaded SETB specimen. (A) Eccentrically loaded SETB specimen, (B) Corresponding load-displacement response, (C) Evolving displacement magnitude with crack growth. The P and Δ values have been normalized with fixed reference values.
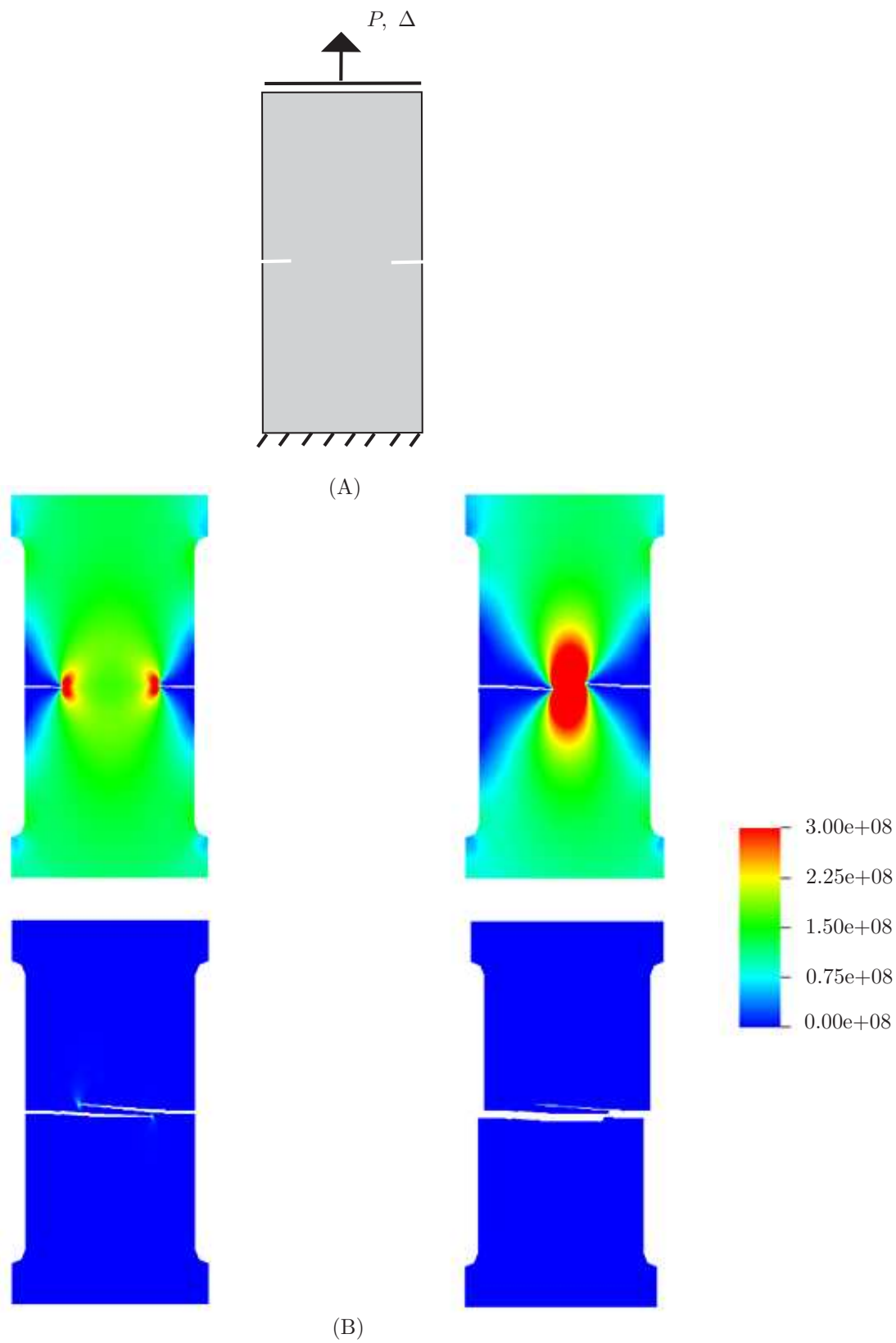
American Institute of Aeronautics and Astronautics
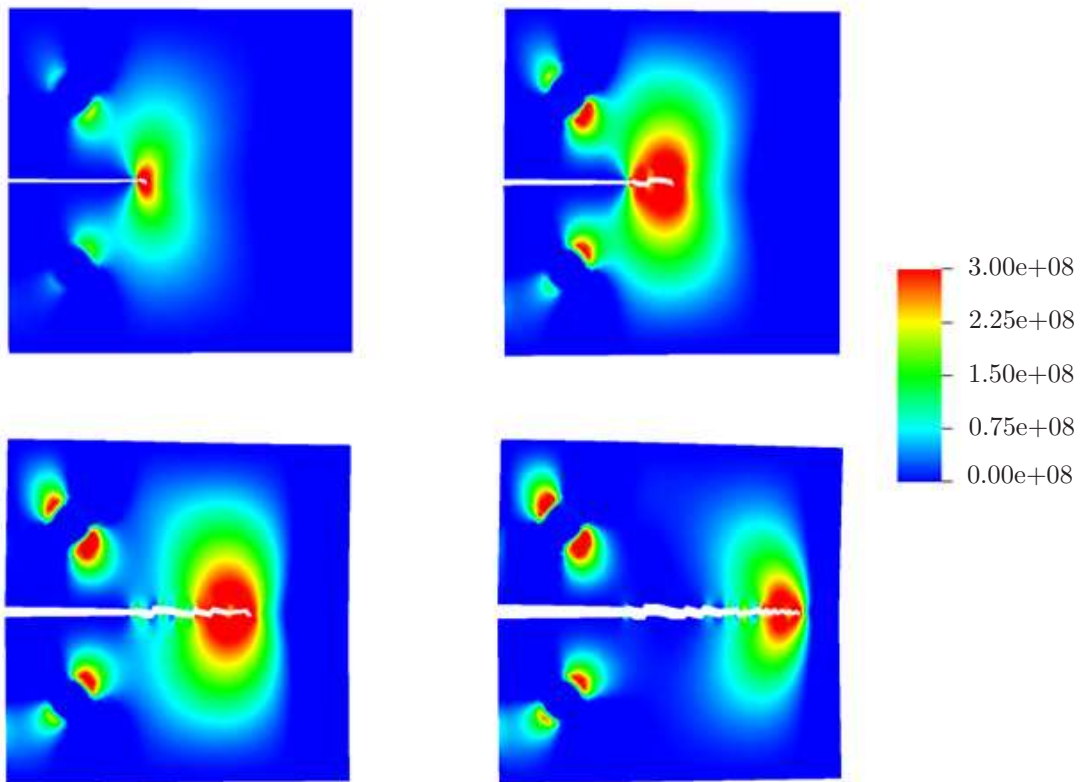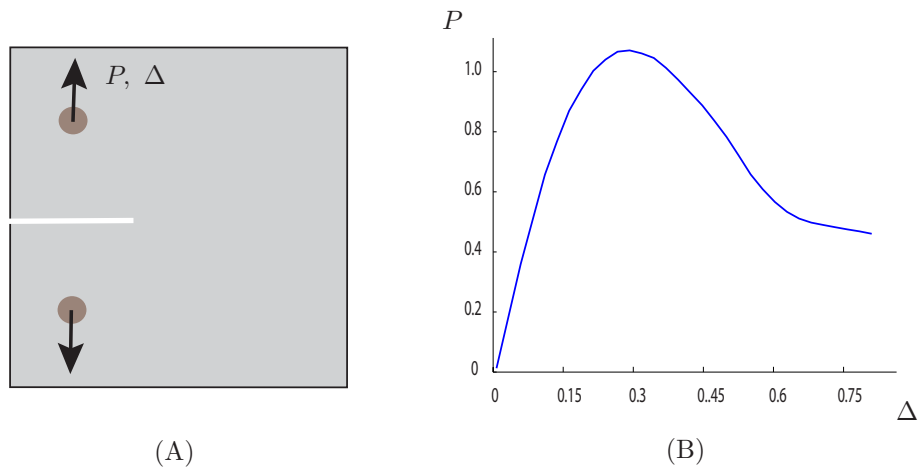
Figure 14. Mixed-mode crack propagation in an symmetrically loaded CTS specimen(A) CTS specimen, (B) Corresponding load-displacement response., (C) Evolving opening stress σ_{yy} magnitude with crack growth. The P and Δ values have been normalized with fixed reference values.

Figure 15. Cohesive crack propagation in DENT specimen. (A) DENT specimen, (B) Evolving opening stress σ_{yy} magnitude with crack growth
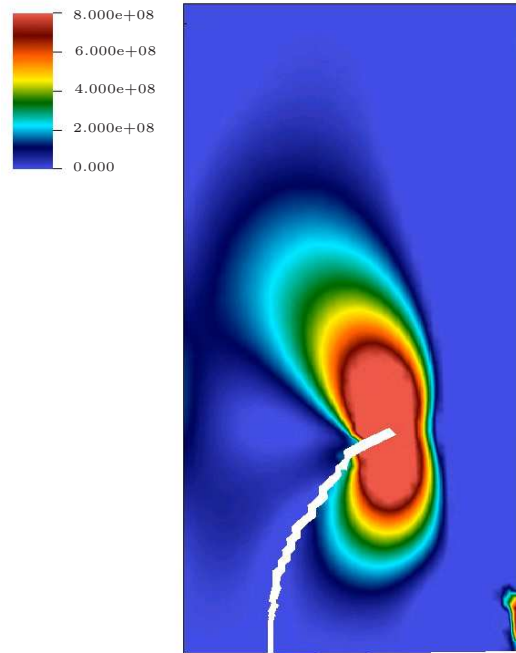
Figure 16. Mixed-mode crack propagation in a rectangular specimen with the left end fully constrained and a displacement loading at the lower right corner. Shown are the crack path and the opening stress contours.
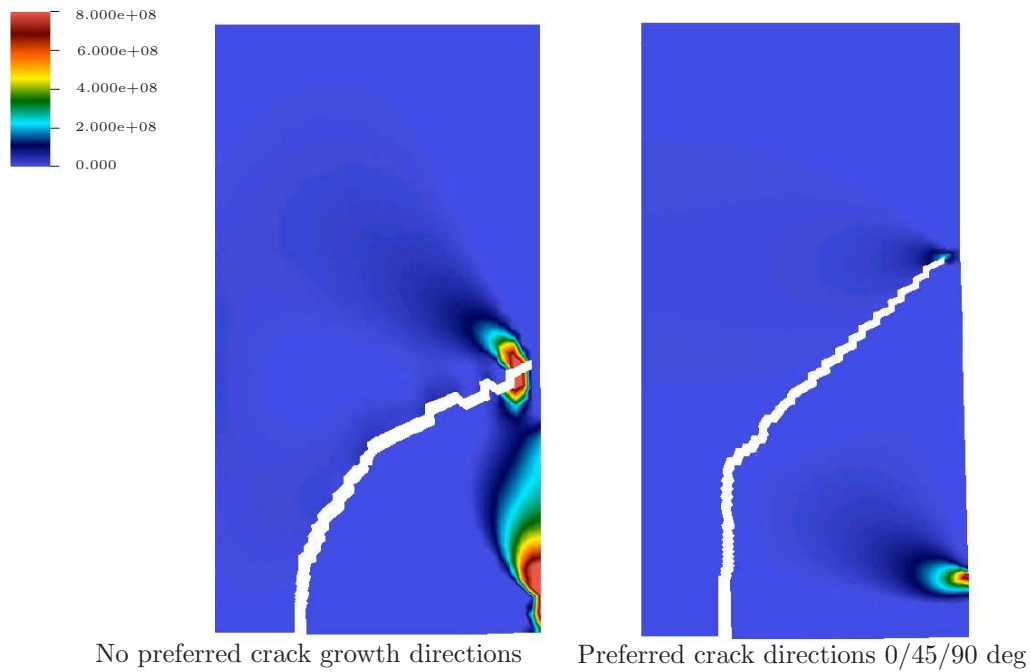

No preferred crack growth directions   Preferred crack directions 0/45/90 deg

Figure 17. Mixed-mode crack propagation with restricted crack growth directions in a rectangular specimen with the left end fully constrained and a displacement loading at the lower right corner. Shown are the crack path and the opening stress contours.
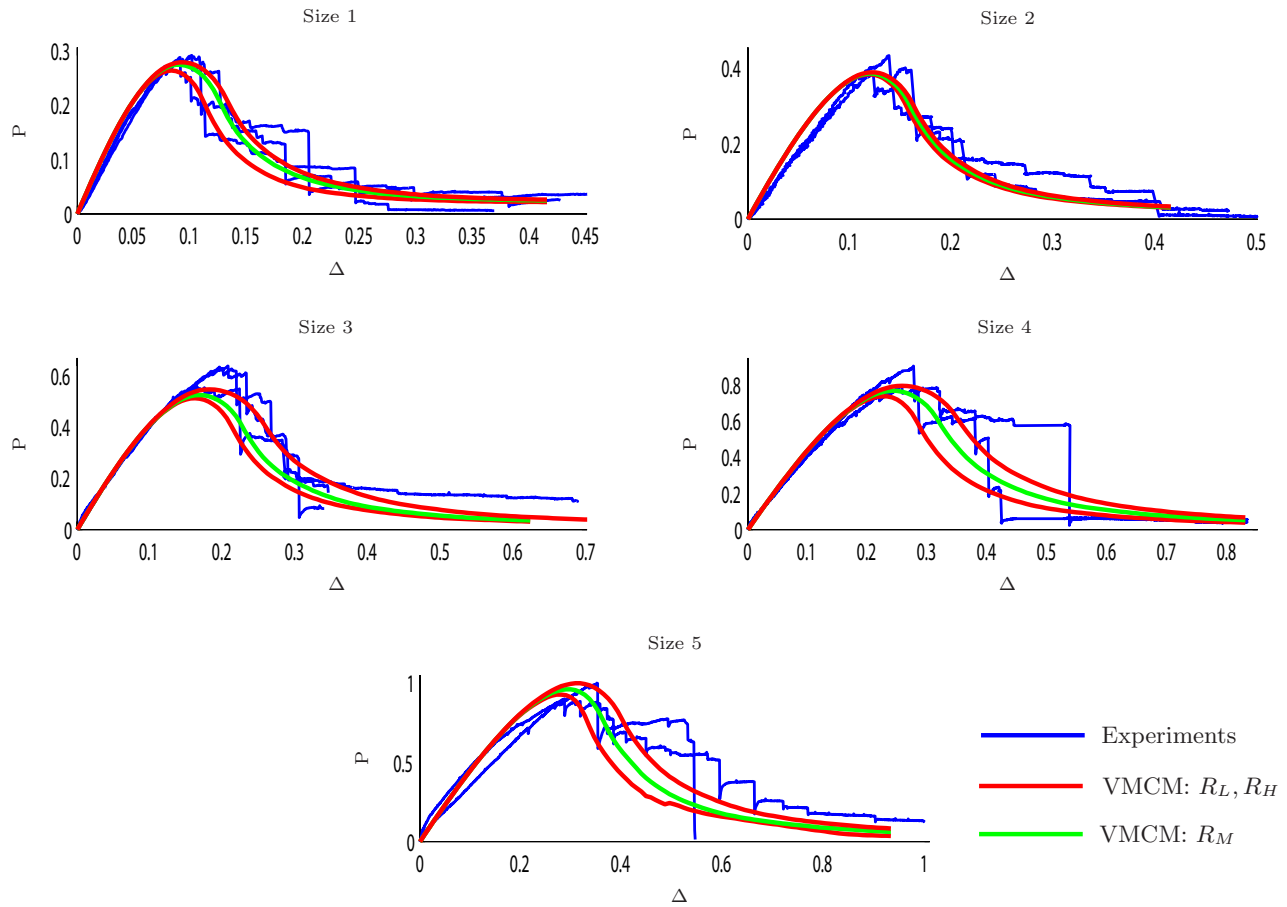
American Institute of Aeronautics and Astronautics

Figure 18. Load-Displacement ($P\Delta$) response obtained from multiscale (VMCM) simulations of symmetrically loaded Size 1-5 SETB specimens with experimentally determined $\mathscr{R}_{avg}$ values (Table 2), compared to their respective experimental curves. For a particular specimen size, R_L and R_H are the least and highest values of fracture resistance obtained from the multiple experimental $P\Delta$ curves, R_M is the average of the fracture resistance of each of the multiple experimental $P\Delta$ curves. R_L corresponds to the curve exhibiting least toughness and R_H corresponds to the curve exhibiting the highest toughness. The P and Δ values have been normalized with fixed reference values.
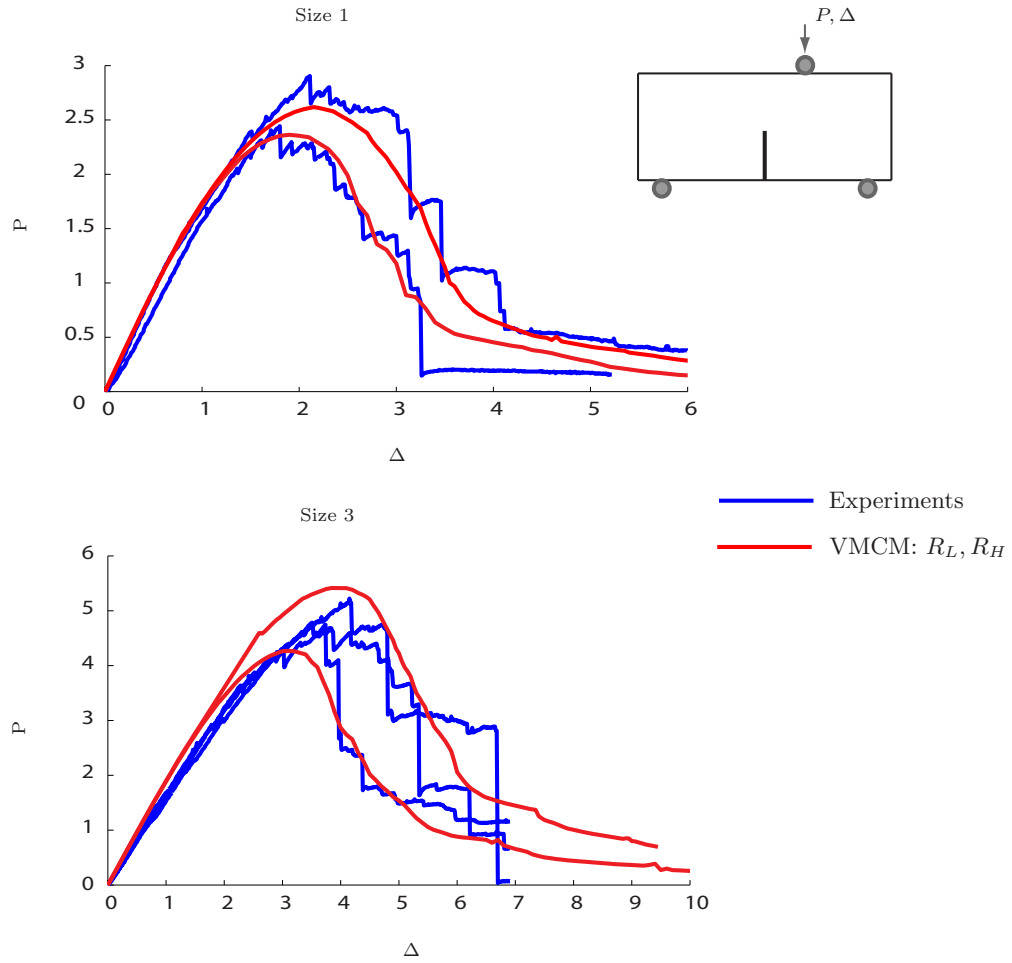
Figure 19. Load-Displacement ($P\Delta$) response obtained from multiscale (VMCM) simulations of eccentrically loaded Size 1,3 SETB specimens with experimentally determined $\mathscr{R}_{avg}$ values (Table 2), compared to their respective experimental curves. For a particular specimen size, R_L and R_H are the least and highest values of fracture resistance obtained from the multiple experimental $P\Delta$ curves. R_L corresponds to the curve exhibiting least toughness and R_H corresponds to the curve exhibiting the highest toughness. The P and Δ values have been normalized with fixed reference values.

American Institute of Aeronautics and Astronautics
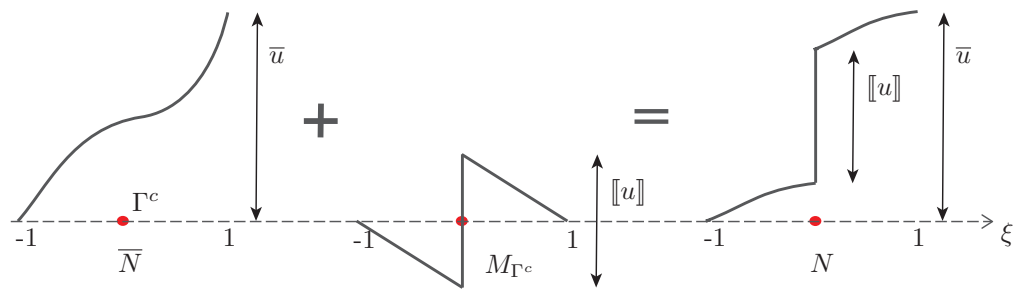
Elemental enrichment (Multiscale)
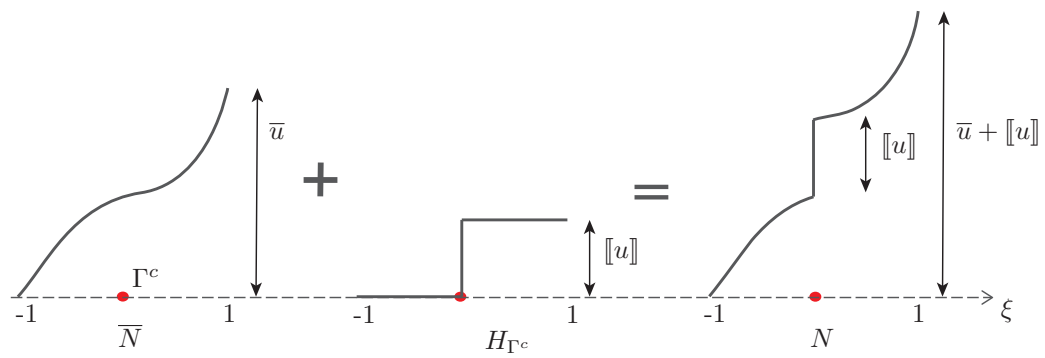
Nodal enrichment

Figure 20. Comparison of the interpolation schemes used to represent the crack surface in the multiscale approach presented here and the other nodal enrichment based approaches.

American Institute of Aeronautics and Astronautics